Soft X-Ray Backlighting of Cryogenic Implosions Using a Narrowband Crystal Imaging System

Introduction

Backlighting is a powerful technique used to observe the flow of dense and relatively cold material in high-energy-density-plasma experiments. This technique has been used successfully in both direct-[1] and indirect-drive[2] inertial confinement fusion implosion experiments to measure the velocity and uniformity of the imploding shell. High-performance, direct-drive cryogenic deuterium–tritium (DT) implosions[3] are a challenging backlighting configuration because of the low opacity of the DT shell, the high shell velocity, the small size of the stagnating shell, and the very bright self-emission of the hot core. A relatively low backlighter photon energy of <2 keV is required to obtain an observable contrast of the backlit images. At a maximum speed of up to 400 μm/ns, backlighting with a nanosecond laser pulse and a conventional x-ray framing camera[4] with an ~40-ps temporal resolution would lead to an ~20-μm motion blurring of the order of the shell's in-flight thickness. For high-performance DT implosions on OMEGA,[5] the size of the hot spot is typically ~20 μm, the temperature >3 keV, and the emission time of the order of 100 ps (Ref. 6), which generates extremely bright self-emission.

A crystal imaging system with a backlighter driven by a short-pulse, high-energy petawatt (HEPW) laser such as OMEGA EP[7] is well suited for backlighting cryogenic DT implosions because of its narrow spectral width, high-throughput, high spatial resolution of the imager, and short emission time and high brightness of the backlighter. Early proof-of-principle experiments on OMEGA using a crystal imaging system and a backlighter driven by the OMEGA EP short pulse[8] laser were performed using room-temperature CH targets. These experiments showed encouraging results with the backlighter intensity within a factor of 2 of the time-integrated core emission and a signal-to-background ratio of >10. The initial data indicated that significant improvements were required in the setup to be able to backlight cryogenic DT targets. The images showed significant astigmatism, which must be reduced. The self-emission of a DT cryo target is orders of magnitude larger compared to a CH target because of the much lower opacity, which requires a time-gated detection system. The backlighter target must be close to the primary target (~5 mm) to achieve the required brightness, which is not compatible with the cryogenic shroud setup on OMEGA.[9]

This article describes the setup of a crystal imaging system for cryogenic DT implosions on OMEGA based on the design presented in Ref. 8. Three major improvements have been implemented: (1) the x-ray reflecting crystal has been mounted on an aspheric substrate to reduce the astigmatism; (2) a time-gated detector has been implemented to record the image; and (3) a fast target-insertion system has been built to insert the backlighter target close to the implosion target within 100 ms after the cryogenic shroud has been removed. The backlighter target material was changed from Si-coated Al foils to pure Si wafers, and the CH filters were replaced with Be filters to increase the brightness of the backlighter and the transmission of the imaging system.

Setup of the Crystal Imaging System

The cryogenic backlighting system uses the Si He$_\alpha$ line at ~1.865 keV (0.664 nm) from a Si backlighter driven by the OMEGA EP laser (see Fig. 139.25). The backlighter target is a 500-μm-sq × 10-μm-thick silicon wafer placed 5 mm from the primary target. A 25-mm-diam quartz crystal, cut
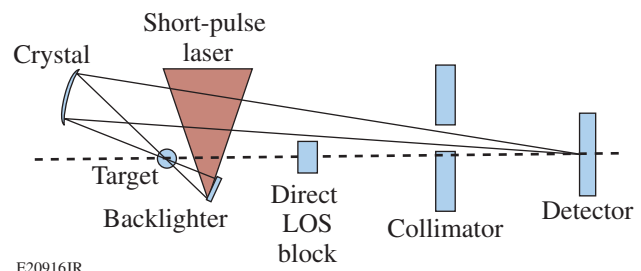

E20916JR

Figure 139.25
Schematic of the spherical crystal imager backlighting setup (not to scale). The short-pulse laser illuminates a backlighter foil behind the primary target, which is heated by 60 beams from the OMEGA laser (not shown). A direct line-of-sight (LOS) block and a collimator protect the detector from background x rays emitted by the backlighter and primary targets.

along the 1011 planes with a $2d$ spacing of 0.6687 nm, is set up so that the x rays from the backlighter are incident on the crystal at 83.9° from the surface—the Bragg angle for the Si He$_\alpha$ line. The crystal is bonded by INRAD[10] to a substrate with a 500-mm major radius of curvature by optical contact. It is placed 267 mm from the implosion target. The image is recorded on a detector located ~3.65 m from the target at a magnification of ~15×. A direct line-of-sight (LOS) block and a collimator are used to protect the detector from background x rays emitted by the backlighter and the primary targets. A 12.5-μm-thick Be foil is used as a blast shield in front of the crystal, and a second 12.5-μm-thick Be foil acts as a light-tight filter in front of the detector. The Be foil in front of the crystal is backed with a stainless-steel mesh to increase its mechanical stability. This system is described in more detail in Ref. 8.

1. Astigmatism-Corrected Crystal Substrates

An aspheric substrate was designed to reduce the optical aberrations of the imager seen in the previous experiments,[8] which are predominantly astigmatism. The deviation from a spherical surface was described in polynomial form (only the five leading terms are shown):

$$z = \frac{\dfrac{x^2 + y^2}{r}}{1 + \sqrt{1 - \dfrac{x^2 + y^2}{r}}}$$

$$+ y^2 A_{2,2} + x^2 A_{2,0} + x^2 y A_{3,1} + y^3 A_{3,3} + x^4 A_{4,0}.$$

A ray-tracing software (FRED)[11] was used to optimize the coefficients for the smallest spot size. The ray-tracing software was set up to use the rocking curve of the crystal as an additional constraint. The width of the rocking curve was set to be 2× the vendor specification of 12 arcsec. The optimized coefficients are listed in Table 139.I. The calculated point-spread func-

Table 139.I: Polynomial coefficients for the optimized aspherical substrate.

i	j	A_{ij}	Polynomial
2	0	8.682×10^{-8}	X^2
2	2	1.140×10^{-5}	Y^2
3	1	-1.545×10^{-7}	$X^2 Y$
3	3	-1.131×10^{-7}	Y^3
4	0	5.372×10^{-10}	X^4

tion (PSF) for this design has a full width at half maximum (FWHM) of ~0.5 μm in the horizontal direction and ~2 μm in the vertical direction (see Fig. 139.26). While it is theoretically possible to calculate a surface prescription that produces a spot with submicron spatial resolution on axis, the polynomial was truncated to stay within the capabilities of the manufacturing process. The substrate was manufactured by QED Technologies[12] to a figure error of 25-nm peak-to-valley and 2-nm root mean square (rms).
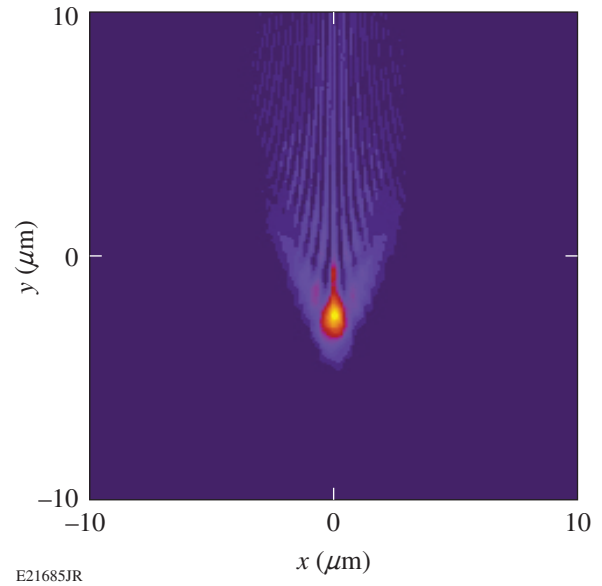

E21685JR

Figure 139.26
Point-spread function (PSF) of the imaging system with an optimized substrate as calculated by FRED.

2. Time-Gated Detector

To reduce the impact of the self-emission of the hot core of the cryo DT implosion, the time-integrated image-plate (IP) detector described in Ref. 8 was replaced by the head of an x-ray framing camera (XRFC)[4] (see Fig. 139.27). The XRFC head was attached at the back of a ten-inch manipulator (TIM-4) with an adapter flange. Slots were cut in the collimator holder to pump out the volume where the microchannel plate (MCP) of the XRFC head operates. A vacuum gauge was used to interlock the high-voltage system of the XRFC head to prevent discharges. The Be filter used to block the UV light from the laser was mounted behind the collimator. The XRFC head was run with a single-strip MCP detector, fed by a 300- to 500-ps-long high-voltage pulse. The image is recorded on film. The spatial resolution of the XRFC recording system is typically ~20 lp/mm (Ref. 13).
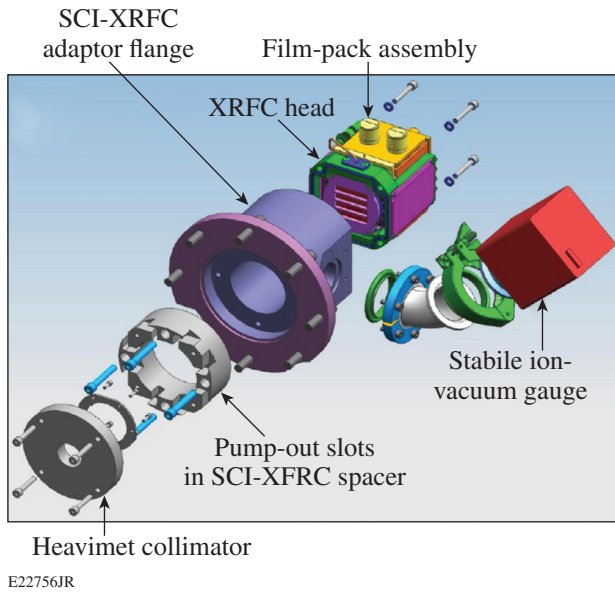
SCI-XRFC adaptor flange

Film-pack assembly

XRFC head

Stabile ion-vacuum gauge

Pump-out slots in SCI-XFRC spacer

Heavimet collimator

E22756JR

Figure 139.27
CAD model of the x-ray framing-camera setup. SCI-XFRC: spherical crystal imaging x-ray framing camera.

3. Fast Target Inserter

Given the available energy of the short-pulse laser system, the backlighter target must be positioned close to the cryo target to maximize the brightness of the backlighter emission. Previous experiments[8] have shown that with a distance of 5 mm for the backlighter target, adequate brightness and backlighter uniformity can be achieved. Unfortunately, this backlighter location is inside the cryogenic shroud system, which protects the cryogenic DT target, being held at a temperature of <20 K,

from ambient thermal radiation.[9] It is impossible to mount the backlighter target on the same support structure as the cryo target since it would distort the uniformity of the isotherms inside the layering sphere, which is essential for obtaining high-quality DT ice layers. A fast target positioner (FASTPOS) was designed to insert the backlighter target after the cryogenic shroud was removed, immediately before the target shot. The timing of the shroud removal leaves an ~100-ms window to insert the backlighter. Given the shroud diameter of ~100 mm and a clearance requirement of ~25 mm around the shroud for the fast retraction operation, a travel distance of ~80 mm is required [see Fig. 139.28(a)].

The design of FASTPOS is based on a commercially available linear actuator from LINMOT[14] [see Fig. 139.28(b)]. This motor is capable of a peak force of ~70 N, providing an acceleration of >10 g, with a moving mass of ~120 g. This actuator was set up in a mounting system with aluminum extensions for the slider, polymer bushings to provide a radial constraint, and a pin-in-slot system to provide a rotational constraint. A Micro-E optical encoder provides high-resolution feedback for a closed-loop control system. Special care was taken to provide a low-resistance ground path for the return current generated by the short-pulse laser interacting with the backlighter target. Extensive tests have shown that the FASTPOS system can insert targets over a distance of ~80 mm, with a final positioning accuracy of <50 μm in ~70 ms. It is very resilient to the electromagnetic interference caused by the short-pulse laser. The instrument performed well and without issues even at the highest laser energies of 1.25 kJ.

(a)   100 mm   (b)
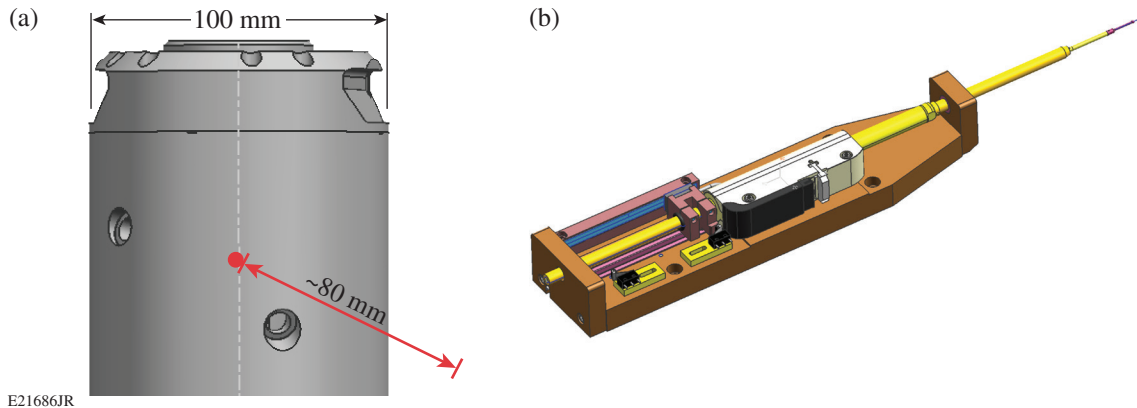
~80 mm

E21686JR

Figure 139.28
(a) Illustration of the path of the backlighter target starting outside the cryo shroud to ~5 mm from the cryo target; (b) CAD drawing of the setup of the fast target positioner (FASTPOS).

Experimental Data

The first experiments with the aberration-corrected cryo-compatible Si He$_\alpha$ spherical crystal imaging (SCI) system were performed using both room-temperature plastic (CH) shells and DT cryogenic targets. Both targets had an 860-μm outer diameter. The CH shells had 27-μm-thick walls, roughly mass equivalent to the cryo DT targets, which had an ~7.5-μm CD outer shell and an ~60-μm-thick DT ice layer. The targets were imploded using ~20 kJ of UV (351-nm) laser light with an ~2- to 3-ns-long highly shaped laser pulse.[3] The backlighter target was made out of a 10-μm-thick Si wafer. The OMEGA EP short-pulse laser illuminated the backlighter foils at an ~45° angle of incidence and focused to an ~350-μm focal spot, corresponding to an average intensity of ~1 × 10^{17} W/cm^2 at 1.25-kJ energy and a 10-ps pulse duration. The OMEGA EP short-pulse laser was fired at various delays of 2 to 3 ns after the start of the OMEGA UV pulse.

1. Gated Imager

A backlit image of (a) a time-integrated cryo DT implosion recorded on an image plate and (b) a time-gated self-emission image recorded on the XRFC are compared in Fig. 139.29. Both images show the emission of the SiC stalk at the bottom of the image that holds the shell. The stalk is irradiated by some of the laser energy that drives the target and emits the same Si He$_\alpha$ radiation as the backlighter. The time-integrated image shows an extremely bright emission peak from the implosion core and a very faint record of the backlighter emission. The core emission saturated the detector and is significantly more than 10× brighter than the backlighter. The time-gated image was recorded without a backlighter using an ~500-ps-long electri-cal gate pulse. The gate pulse was timed to avoid the emission of the core. The image is dominated by the emission from the shell as it is heated by the UV laser. It shows only a very faint signal from the core in the center of the shell, demonstrating the very high extinction ratio of the gated recording system.

2. Performance of the Crystal Imager

Figure 139.30(a) shows a time-gated backlit image from an implosion experiment with a mass-equivalent CH target taken between the end of the drive laser pulse and the start of the self-emission at peak compression. The gate of the XRFC was set to ~300 ps. The emission from the SiC stalk is seen at the bottom of the image. A "shadow" from the highly opaque compressed CH shell is seen in front of the emission from the Si backlighter. Since the gate time was set to start after the end of the laser pulse, no signal from the shell self-emission is visible.

A "cusp"-like feature in the absorption at the bottom of the shadow shows the effect of the stalk and the glue, with which it is attached to the shell, on the implosion dynamics. A second faint absorption feature close to the top of the target image is most likely caused by a piece of debris on the outer shell. This image shows the high optical quality of the improved imaging system; the astigmatism seen in previous experiments is fully corrected. A vertical lineout [Fig. 139.30(b)] is used for a detailed comparison between the measured signal and post-processed one-dimensional (1-D) simulation. The measurements compare very favorably with the simulation in the parts of the shell not influenced by the stalk (top of the target, right side in lineout), showing that the resolution of the imager is good enough to capture the dominant features of the implosion. The
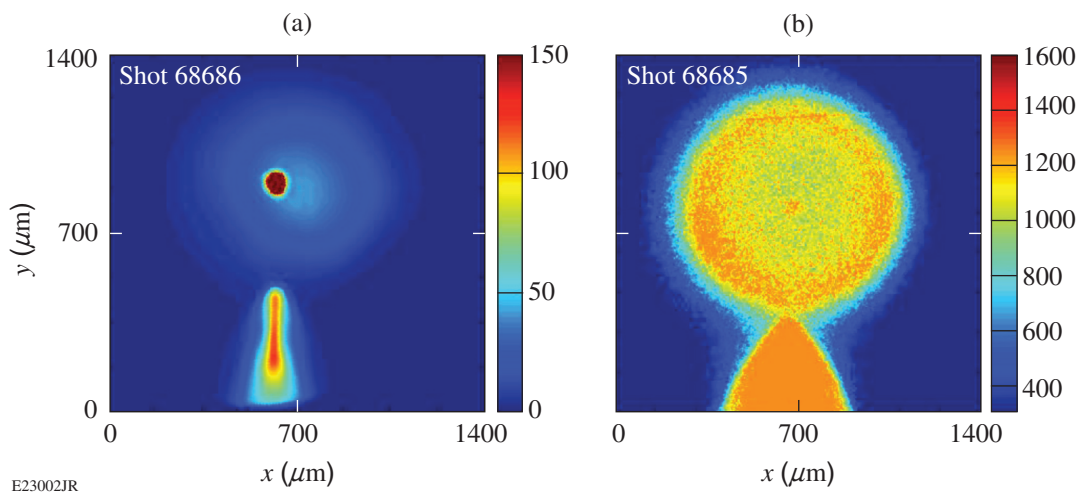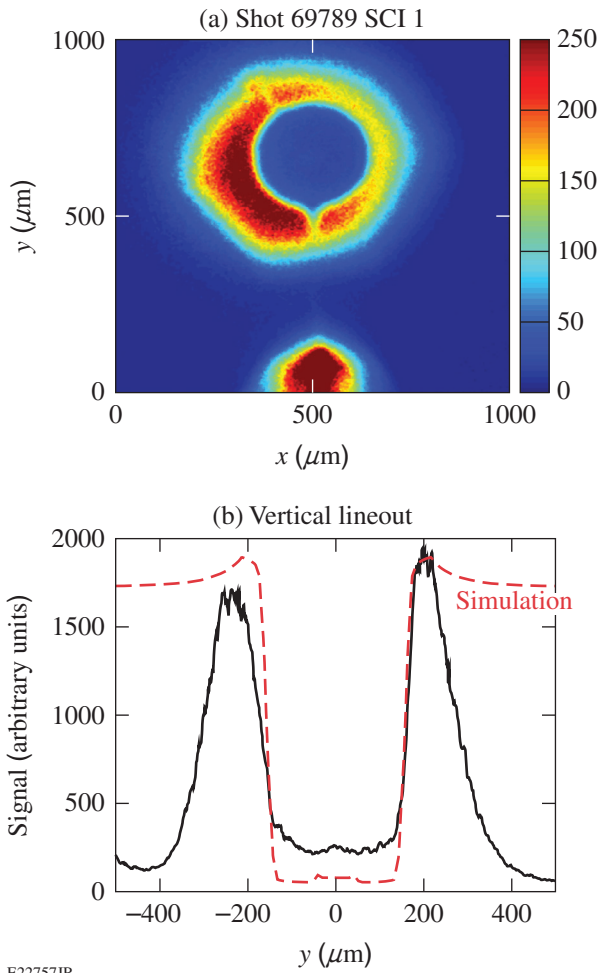

Figure 139.29
(a) Time-integrated image of a backlit DT cryo implosion recorded on an image plate; (b) time-gated image of the self-emission from a DT cryo implosion.
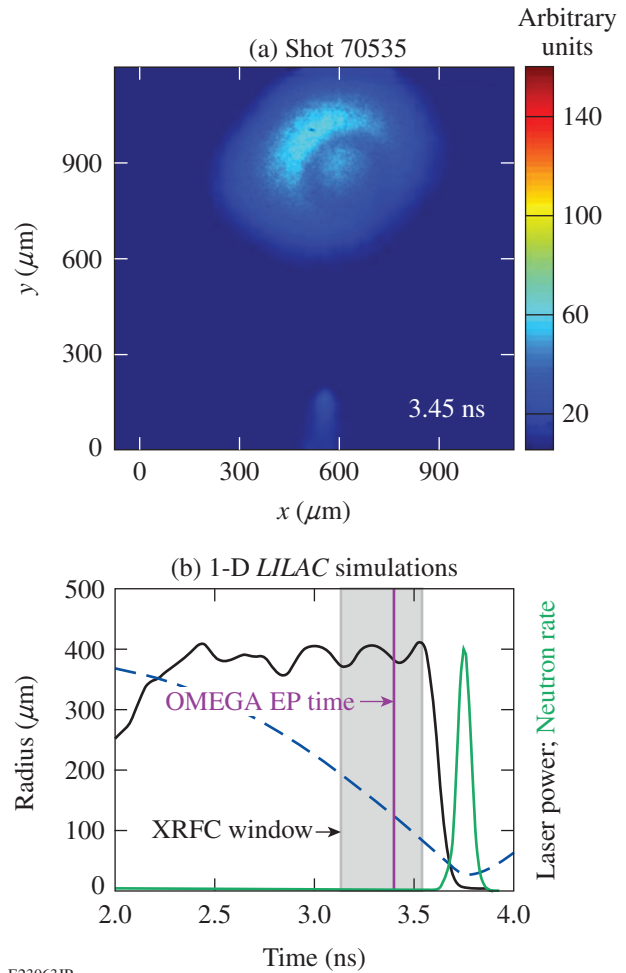
(a) Shot 69789 SCI 1

(b) Vertical lineout

Simulation

E22757JR

Figure 139.30
(a) Time-gated backlit image from a mass-equivalent CH implosion experiment; (b) vertical lineout through the backlit image.

~120 μm. The image shows a faint record of the self-emission of the SiC stalk at the bottom of the target. The shadowgraph of the imploded shell is slightly offset from the center of the backlighter, illustrating the difficulties in aligning the crystal, primary target, and backlighter on a common line of sight. No indication of the self-emission from the shell is seen in the image, showing that the brightness of the backlighter and the narrow spectral acceptance of the imaging system are sufficient to suppress this background source. No bright emission from the core is seen in the center of the absorption feature, demonstrating again that the extinction of the gated imager is good enough to obtain high-quality data.

effect of the stalk is clearly visible in the lineout. More-involved two- (2-D) or three-dimensional (3-D) simulations are required for a detailed analysis of the stalk and debris effects. Shots with a static resolution target in place of the primary target and only the backlighter pulse indicate that the spatial resolution of the imager is ~10 μm at 10% modulation, which is significantly more than the expected resolution of a few microns.

3. Backlit Cryogenic Targets

As expected, the images from cryogenic DT targets show significantly less contrast compared to the mass-equivalent CH targets [see Fig. 139.31(a)]. A 300-ps gate was used in these experiments to minimize the contribution from self-emission. The gate was timed to start ~500 ps before the time of peak core emission [see Fig. 139.31(b)]. The OMEGA EP short-pulse laser was fired ~100 ps before the end of the gate at a time when the shell assembly was compressed to a radius of

(a) Shot 70535

Arbitrary units

3.45 ns

(b) 1-D LILAC simulations

OMEGA EP time →

XRFC window →

E23063JR

Figure 139.31
(a) Time-gated image of a backlit DT cryogenic implosion. (b) Temporal evolution of the shell radius center (blue) compared to the temporal history of the laser power and neutron-production rate from 1-D LILAC simulations for the shot shown in (a). The exposure timing of the XRFC is indicated by the gray-shaded area; the arrival time of the OMEGA EP short-pulse laser is indicated by the purple vertical line.

Image Analysis and Interpretation

To measure the absorption in the compressed shell and quantitatively compare the signal recorded by the crystal imager with simulations, the data must be corrected for the backlighter shape. A simple first-order physical model was constructed to describe the shape of the backlighter by assuming a constant brightness source [see Fig. 139.32(a)]. This source was convolved with a Gaussian PSF, representing the spatial resolution of the imaging system at a 5-mm defocus [Fig. 139.32(b)]. The brightness and extent of the source and the width of the PSF were varied to obtain a best fit to the shape of the measured signal outside the area affected by the absorption of the target. This simple model fits the measured data quite well [see Fig. 139.32(c)].

Figure 139.33 shows a lineout through the image of shot 70535 corrected for the backlighter shape. For comparison, the result from a 1-D *LILAC*[15] hydrocode simulation, post-processed with the radiation transport code *Spect3D*,[16] is plotted (red dotted line). The backlighter timing had to be shifted by ~100 ps earlier to match the measured size of the absorption feature, indicating that the implosion is slightly delayed compared to the simulations.[6] The measured absorption is seen to be much higher than the absorption calculated from the simulations. One possible explanation for this discrepancy is the Rayleigh–Taylor mixing of carbon from the outer CD shell into the DT ice during the shell acceleration. Adding a small amount of carbon uniformly into the shell in the *Spect3D* post-processor[16] [0.1% C (green dashed–dotted line), 0.2% C (blue dashed line)] significantly increases the absorption in the model and brings the simulation much closer to the experimental data, especially in the areas of highest absorption corresponding to the dense shell. In the center of the image the calculated absorption with carbon mixing is higher than observed. This could either be caused by a small amount of self-emission, which is not fully

suppressed by the gating, or be indicative of 3-D effects, like the presence of the nonlinear phase of the Rayleigh–Taylor instability, where large bubbles of the light material (DT) separate thin spikes of the heavy material (carbon). An imaging system with limited resolution looking radially (center of the image) will mostly observe the low absorption of the DT bubbles. At the position of the dense shell, the line of sight of the imager will be predominantly perpendicular to the bubbles and spikes; consequently, the absorption will be influenced more by the high opacity of the carbon spikes. Another possible explanation of the higher-than-predicted absorption could be uncertainties in the opacity models. Further experiments are necessary to separate these issues and more fully understand the measured data.
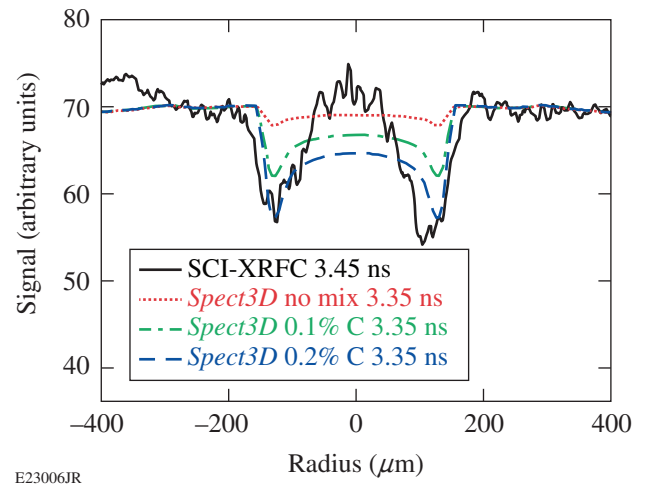
E23006JR

Figure 139.33
Lineout through the backlit image of shot 70535 corrected for the shape of the backlighter emission (black solid line) compared to *Spect3D* post-processed 1-D *LILAC* simulations with varying levels of carbon mixed into the DT shell.
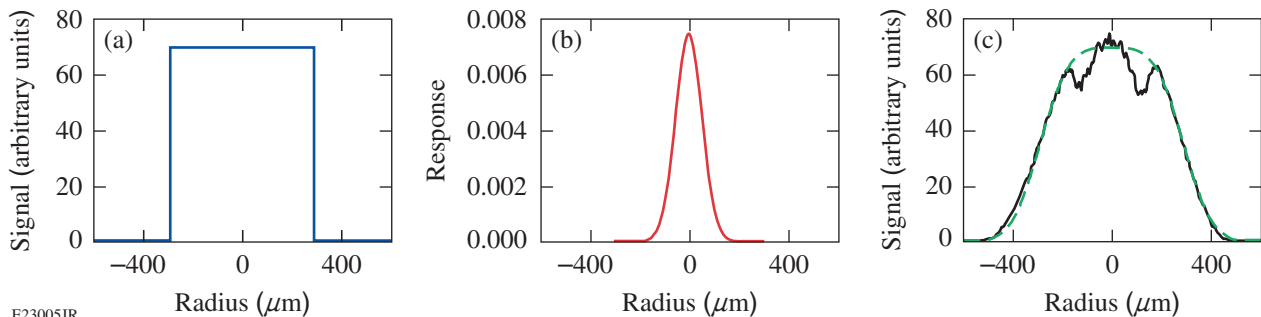
E23005JR

Figure 139.32
(a) A uniform source distribution is convolved with (b) a Gaussian PSF (c) to fit (green line) the measured shape (black line) of the backlighter lineout.

Summary and Outlook

A crystal imaging system capable of backlighting cryogenic implosions using the Si He$_\alpha$ line at ~1.865 keV has been developed on the OMEGA Laser System. Three major improvements were implemented on the previous setup used for proof-of-principle experiments with room-temperature CH targets:[8] (1) The Bragg crystal was bonded to an aspherically shaped substrate, significantly reducing the optical aberrations. (2) A time-gated detector was set up using the head of an XRFC. The background from the very bright emission of the implosion core prominently seen in previous time-integrated experiments was almost completely eliminated. (3) A fast target-insertion system was set up, capable of inserting the backlighter target ~80 mm in <100 ms, which made it possible to perform experiments with a backlighter very close to the cryogenic target (~5 mm) without any modification to the cryogenic layering system, which could have compromised the quality of the DT ice layer.

High-quality backlit images were recorded with this system on cryogenic DT implosions. A simple procedure to correct for the shape of the backlighter based on a physical model of the imager was developed and applied to lineouts from the images. The corrected lineout shows significantly more absorption than a post-processed 1-D hydro simulation of the experiment, which could be an indication of carbon mixing deep into the DT ice layer during the acceleration phase of the implosion.

The resolution of the imaging system is adequate to resolve the spatial structures seen in cryogenic implosions ~200 ps before peak compression, but it might be a limiting factor closer to peak compression, where the spatial scales are compressed by a factor of ~3. The discrepancy between measured and calculated resolution will be studied in offline experiments to explore the causes and potential remedies for this issue.

The description of the backlighter shape could be improved with a higher-order physical model, like the one based on a Taylor expansion,[2] or a decomposition in sinusoidal modes.

ACKNOWLEDGMENT

REFERENCES

1. P. B. Radha, F. J. Marshall, J. A. Marozas, A. Shvydky, I. Gabalski, T. R. Boehly, T. J. B. Collins, R. S. Craxton, D. H. Edgell, R. Epstein, J. A. Frenje, D. H. Froula, V. N. Goncharov, M. Hohenberger, R. L. McCrory, P. W. McKenty, D. D. Meyerhofer, R. D. Petrasso, T. C. Sangster, and S. Skupsky, Phys. Plasmas **20**, 056306 (2013).

2. D. G. Hicks *et al.*, Phys. Plasmas **17**, 102703 (2010).

3. T. C. Sangster, V. N. Goncharov, R. Betti, T. R. Boehly, D. T. Casey, T. J. B. Collins, R. S. Craxton, J. A. Delettrez, D. H. Edgell, R. Epstein, K. A. Fletcher, J. A. Frenje, V. Yu. Glebov, D. R. Harding, S. X. Hu, I. V. Igumenshchev, J. P. Knauer, S. J. Loucks, C. K. Li, J. A. Marozas, F. J. Marshall, R. L. McCrory, P. W. McKenty, D. D. Meyerhofer, P. M. Nilson, S. P. Padalino, R. D. Petrasso, P. B. Radha, S. P. Regan, F. H. Seguin, W. Seka, R. W. Short, D. Shvarts, S. Skupsky, V. A. Smalyuk, J. M. Soures, C. Stoeckl, W. Theobald, and B. Yaakobi, Phys. Plasmas **17**, 056312 (2010).

4. D. K. Bradley *et al.*, Rev. Sci. Instrum. **66**, 716 (1995).

5. T. R. Boehly, D. L. Brown, R. S. Craxton, R. L. Keck, J. P. Knauer, J. H. Kelly, T. J. Kessler, S. A. Kumpan, S. J. Loucks, S. A. Letzring, F. J. Marshall, R. L. McCrory, S. F. B. Morse, W. Seka, J. M. Soures, and C. P. Verdon, Opt. Commun. **133**, 495 (1997).

6. T. C. Sangster, V. N. Goncharov, R. Betti, P. B. Radha, T. R. Boehly, D. T. Casey, T. J. B. Collins, R. S. Craxton, J. A. Delettrez, D. H. Edgell, R. Epstein, C. J. Forrest, J. A. Frenje, D. H. Froula, M. Gatu-Johnson, V. Yu. Glebov, D. R. Harding, M. Hohenberger, S. X. Hu, I. V. Igumenshchev, R. Janezic, J. H. Kelly, T. J. Kessler, C. Kingsley, T. Z. Kosc, J. P. Knauer, S. J. Loucks, J. A. Marozas, F. J. Marshall, A. V. Maximov, R. L. McCrory, P. W. McKenty, D. D. Meyerhofer, D. T. Michel, J. F. Myatt, R. D. Petrasso, S. P. Regan, W. Seka, W. T. Shmayda, R. W. Short, A. Shvydky, S. Skupsky, J. M. Soures, C. Stoeckl, W. Theobald, V. Versteeg, B. Yaakobi, and J. D. Zuegel, Phys. Plasmas **20**, 056317 (2013).

7. C. Stoeckl, J. A. Delettrez, J. H. Kelly, T. J. Kessler, B. E. Kruschwitz, S. J. Loucks, R. L. McCrory, D. D. Meyerhofer, D. N. Maywar, S. F. B. Morse, J. Myatt, A. L. Rigatti, L. J. Waxer, J. D. Zuegel, and R. B. Stephens, Fusion Sci. Technol. **49**, 367 (2006).

8. C. Stoeckl, G. Fiksel, D. Guy, C. Mileham, P. M. Nilson, T. C. Sangster, M. J. Shoup III, and W. Theobald, Rev. Sci. Instrum. **83**, 033107 (2012).

9. *LLE Review Quarterly Report* **81**, 6, Laboratory for Laser Energetics, University of Rochester, Rochester, NY, LLE Document No. DOE/SF/19460-335 (1999).

10. INRAD Optics, Northvale, NJ 07647.

11. Photon Engineering, accessed 9 April 2012, http://www.photonengr.com.

12. Q22, QED Technologies, LLC, Rochester, NY 14607.

13. J. A. Oertel, T. Archuleta, C. G. Peterson, and F. J. Marshall, Rev. Sci. Instrum. **68**, 789 (1997).

14. NTI AG - LinMot & MagSpring, CH-8957 Spreitenbach, Switzerland.

15. J. Delettrez, R. Epstein, M. C. Richardson, P. A. Jaanimagi, and B. L. Henke, Phys. Rev. A **36**, 3926 (1987).

16. Prism Computational Sciences, Inc., Madison, WI 53711.